J Nanostruct 16(3): 3217-3226, Summer 2026

RESEARCH PAPER

Nanocrystalline Cu(II) Schiff-Base/Viologen Adducts: Williamson-Hall Size-Strain Analysis and Redox-Triggered π-Dimer Molecular Switches

Khalid K. Shaker, Wathiq S. Abdul-Hassan*, Athraa H. Mekky

Department of Chemistry, College of Science, University of Thi-Qar, Thi-Qar 64001, Iraq

ARTICLE INFO

Article History:
Received 19 March 2026
Accepted 10 May 2026
Published 01 July 2026

Keywords:
Chlorinated Schiff base
Lattice strain
Nanocrystalline copper complexes
Williamson–Hall
π-Dimerization

ABSTRACT

A new family of nanocrystalline copper(II) bis(keto-imino) complexes bearing the chlorinated Schiff-base ligand (Z)-ethyl 4-chloro-3-(phenylimino)butanoate (EClN) was synthesized and structurally characterized at the nanoscale. The parent complex CuEClN was prepared by condensation of EClN with copper(II) acetate, then five-coordinate adducts CuEClN-py, CuEClN-bpy, CuEClN-$C_1V^+.PF_6^-$ and CuEClN-$V_2^{2+}.2PF_6^-$ were obtained through axial coordination of pyridine, 4,4'-bipyridine, mono-methyl viologen hexafluorophosphate ($C_1V^+.PF_6^-$) and propylene-bridged bis-viologen bis(hexafluorophosphate) ($V_2^{2+}.2PF_6^-$). The compounds were identified by FT-IR, LC-MS, UV-Visible and TGA analyses. Powder X-ray diffraction confirmed the crystalline character of every compound, and crystallite sizes were quantified in the nanoscale (range ≈ 6 – 81 nm) by both Scherrer and Williamson–Hall (W–H) models. The W–H analysis simultaneously delivered the lattice-strain (ε) and revealed that bulky charged axial viologens generate the strongest distortion ($\varepsilon = 1.56 \times 10^{-3}$ for CuEClN-$V_2^{2+}.2PF_6^-$), whereas the small, flexible parent ligand EClN gives the most ordered lattice. FE-SEM micrographs corroborated the XRD trend: chlorinated viologen complexes display sub-10 μm aggregates with finer secondary particles. UV-Visible spectra in DMF/DMSO show the d–d transitions expected for square-planar (CuEClN) and square-pyramidal (adducts) geometries. Chemical reduction of the viologen-bearing complexes by activated zinc and electrochemical reduction by cyclic voltammetry in DMF (under Ar) furnished, respectively, intermolecular π-dimers $(CuEClNC_1V\bullet)_2$ and an intramolecular bis-viologen π-dimer within $CuEClNV_2$, monitored by characteristic absorption bands at ≈ 380 nm and ≈ 554–560 nm. The reversibility upon air re-oxidation establishes these nanocrystalline complexes as redox-triggered molecular switches and promising candidates for nano-electronic and smart-material applications.

How to cite this article
K. Shaker KH, S. Abdul-Hassan W, H. Mekky A. Nanocrystalline Cu(II) Schiff-Base/Viologen Adducts: Williamson-Hall Size-Strain Analysis and Redox-Triggered π-Dimer Molecular Switches. J Nanostruct, 2026; 16(3):3217-3226. DOI: 10.22052/JNS.2026.03.018

* *Corresponding Author Email: Wathiq-a.chem@sci.utq.edu.iq*

INTRODUCTION

Nanocrystalline coordination compounds occupy a privileged position at the interface between molecular chemistry and materials science: their physical properties (optical, redox, magnetic, thermal) emerge not only from the molecular architecture, but also from the size and strain of the crystallites that they form in the solid state. For copper(II) β-diketonate frameworks in particular, the cooperative behaviour between coordinated metal centre, chelating ligand and bulky axial donor controls both the intramolecular electronic structure and the inter-molecular packing geometry that governs nano-domain formation [1–4].

Among redox-active building blocks, viologen (4,4′-bipyridinium) derivatives are unique. The dication V^{2+} is reduced reversibly to a violet radical cation $V^{\bullet+}$ that, at sufficient concentration, dimerizes through non-covalent π–π interaction to a diamagnetic π-dimer $(V)_2^{2+}$ [5–7]. When two viologen radicals are tethered through a flexible spacer or coordinated as axial ligands to a Cu(II) centre, the dimerization can be intramolecular (within a single molecule) or intermolecular (between two complex units). This switchable contraction–elongation has motivated their incorporation into electrochromic devices, redox-flow batteries and molecular memory elements [8–11].

Schiff bases derived from β-keto-esters and primary amines are an attractive equatorial scaffold for Cu(II): they enforce a robust square-planar N_2O_2 chelate, leave the axial positions of Cu(II) accessible to a fifth donor, and deliver photophysical signatures that report on coordination changes [12–15]. Halogenation of the ester moiety (replacing the methyl by a chloromethyl group) modifies both the steric profile and the local dipole, and consequently the crystal packing and lattice strain [16,17]. Yet no systematic, nano-scale structural investigation of chlorinated Cu(II) bis(keto-imino) complexes carrying axial mono- or bis-viologen units has been reported.

In the present work we (i) synthesized the chlorinated Schiff base (Z)-ethyl 4-chloro-3-(phenylimino)butanoate (EClN), its parent complex CuEClN and four axially coordinated adducts with pyridine, 4,4′-bipyridine, $C_1V^+.PF_6^-$ and $V_2^{2+}.2PF_6^-$; (ii) extracted nanocrystalline parameters — average crystallite size D and microstrain ε — from powder XRD using both Scherrer and Williamson–Hall models, and correlated them with the size, charge and rigidity of the axial donor; (iii) corroborated the W–H trend by FE-SEM imaging at the nano/micro scale; and (iv) demonstrated, by chemical reduction with activated zinc and by cyclic voltammetry, the operation of redox-triggered π-dimerization switches centred on the axial viologen, monitored in real time by UV-Visible spectroscopy.

MATERIALS AND METHODS

Materials and instrumentation

Aniline, ethyl 4-chloroacetoacetate, copper(II) acetate monohydrate, pyridine, 4,4′-bipyridine, methyl iodide and 1,3-dibromopropane were of analytical grade and used as received. Solvents (ethanol, methanol, DMF, DMSO, DCM, acetonitrile, diethyl ether) were used without further purification. KPF_6 was supplied by Sigma-Aldrich. FT-IR spectra were recorded on a Perkin-Elmer Tensor-27 (Bruker) spectrometer using KBr discs in the 4000–400 cm^{-1} range (Department of Chemistry, University of Thi-Qar). ^{1}H-NMR spectra were measured on a Bruker Ascend 400 MHz instrument in DMSO-d_6 (College of Education for Pure Sciences, University of Basrah). LC-MS spectra were acquired on an Agilent 5973 Network MS detector (EI, 70 eV; mobile phase MeOH/H_2O) at the University of Tehran. UV-Visible spectra were measured on a PG-Instruments T90+ spectrophotometer using a 1 cm quartz cell. Thermogravimetric and DTA traces were recorded on a TA SDT Q600 instrument at a heating rate of 10 °C min^{-1} in air or argon. Powder XRD patterns were collected on a PANalytical diffractometer using Cu Kα radiation (λ = 1.5405 Å) over 2θ = 5–80°. Field-emission scanning electron microscopy (FE-SEM) and EDS measurements were performed at 20 kV at the University of Tehran. Cyclic voltammetry was carried out on a PARSTAT 4000 (AMETEK, France) under argon at room temperature, using a three-electrode cell (3 mm vitreous carbon working electrode, Pt wire counter, Ag pseudo-reference) in DMF + 0.1 M tetra-n-butylammonium perchlorate (TBAP) at 100 and 300 mV s^{-1}.

Synthesis of the viologen building blocks

$C_1V^+.PF_6^-$ and $V_2^{2+}.2PF_6^-$ were prepared in two steps following the reported procedure [11,12]. Briefly, methyl iodide (0.39 mL, 6.4 mmol) was added to 4,4′-bipyridine (1.0 g, 6.4 mmol) in 10

mL of DCM and stirred at room temperature for 24 h. The yellowish-orange solid was filtered and recrystallized from methanol to give $C_1V^+.I^-$ (1.0 g, 61 %, m.p. 248 °C). Anion exchange in water with saturated aqueous KPF_6 furnished $C_1V^+.PF_6^-$ as a white precipitate. The bis-viologen $V_2^{2+}.2Br^-$ was obtained from 4,4′-bipyridine (2.0 g, 12.8 mmol, 2 eq) and 1,3-dibromopropane (0.65 mL, 6.4 mmol, 1 eq) in 20 mL of acetonitrile at 70 °C for 24 h, and then converted to $V_2^{2+}.2PF_6^-$ by anion exchange (yield 1.0 g, 48 %).

Synthesis of (Z)-ethyl 4-chloro-3-(phenylimino) butanoate (EClN)

Freshly distilled aniline (2 mL, 2.06 g, 0.022 mol, 1 eq) was added drop-wise to a solution of ethyl 4-chloroacetoacetate (2.90 mL, 0.020 mol, 1 eq) in absolute ethanol. The mixture was refluxed for 6 h and the progress monitored by TLC (ethyl acetate/ benzene 4:6). The crude oil was air-dried and recrystallized from benzene/hexane (1:1) to afford EClN as a dark-brown solid. Yield: 3.0 g, 68 %; m.p. 160 °C; soluble in EtOH, MeOH, DCM, DCE, $CHCl_3$, acetone, benzene, DMF and DMSO; insoluble in n-hexane. UV-Vis (DMF, 0.02 mM): λ_max / nm (ε / M^{-1} cm^{-1}) = 303 (11 450), 427 (1 100). FT-IR (KBr, cm^{-1}): 3041 ν(=C–H); 2929, 2900, 2830 ν(C–H); 1733 ν(C=O); 1696 ν(C=N); 1614–1495 ν(C=C); 1220–1027 ν(C–O). ^{1}H-NMR (400 MHz, DMSO-d_6): δ / ppm = 7.5 (d, 2H), 7.4 (d, 2H), 7.5 (t, 1H), 4.1 (s, 2H, $ClCH_2$), 3.4 (q, 2H), 1.1 (t, 3H).

Synthesis of CuEClN

Copper(II) acetate (0.44 g, 2.21 mmol, 1 eq) dissolved in 20 mL of methanol/water (1:1) was added drop-wise over 15 min to EClN (1.0 g, 4.44 mmol, 2 eq). The mixture was refluxed for 4 h. The black precipitate was collected by filtration, washed with water and methanol, and dried under vacuum. Yield: 1.05 g, 47.7 %; m.p. 230 °C; soluble in DMF and DMSO. UV-Vis (DMF, 0.1 mM): λ_max / nm (ε) = 279 (11 030), 355 (6 110), 374 (3 001); at 1 mM: 430 (2 112), 567 (1 184). FT-IR: 3045–3030 ν(=C–H); 2981–2928 ν(C–H); 1733 ν(C=O); 1695 ν(C=N); 1646–1493 ν(C=C); 1200–1043 ν(C–O); 696–509 ν(Cu–O), ν(Cu–N).

Synthesis of CuEClN-py

Pyridine (1.1 mL, 0.0129 mol, 20 eq) was added to CuEClN (0.35 g, 0.63 mmol, 1 eq) in 3 mL of DMF. The mixture was stirred at room temperature for 48 h. The black precipitate was filtered, washed with DCM, methanol and ethanol, and dried under vacuum. Yield: 0.35 g, 30 %; m.p. 280 °C (dec.). UV-Vis (DMSO, 0.04 mM): λ_max / nm (ε) = 273 (11 702), 392 (4 852); at 0.1 mM: 266 (97 050), 391 (51 100), 866 (37). FT-IR: 3045 ν(=C–H); 2980–2855 ν(C–H); 1734 ν(C=O); 1695 ν(C=N); 1647–1493 ν(C=C); 1200–1043 ν(C–O); 696–506 ν(Cu–O), ν(Cu–N).

Synthesis of CuEClN-bpy

4,4′-Bipyridine (0.30 g, 1.9 mmol, 3 eq) was added to CuEClN (0.35 g, 0.74 mmol, 1 eq) in 3 mL of DMF. The mixture was stirred at room temperature for 48 h. The black precipitate was collected, washed with DCM and methanol, and dried under vacuum. Yield: 0.30 g, 50 %; m.p. 292 °C (dec.). UV-Vis (DMF, 0.04 mM): λ_max / nm (ε) = 272 (24 780), 362 (7 225); at 1 mM: 463 (2 301), 557 (1 382). FT-IR: 3063 ν(=C–H); 2980–2933 ν(C–H); 1665 ν(C=N); 1547–1496 ν(C=C); 1226–1027 ν(C–O); 760–511 ν(Cu–O), ν(Cu–N).

Synthesis of CuEClN-$C_1V^+.PF_6^-$

$C_1V^+.PF_6^-$ (0.74 g, 3 eq) was added to CuEClN (0.40 g, 0.74 mmol, 1 eq) in 3 mL of DMF and stirred at room temperature for 30 days. The black precipitate was collected, washed with DCM, methanol and ethanol, and dried under vacuum. Yield: 0.40 g, 50 %; m.p. 250 °C. UV-Vis (DMF, 0.1 mM): λ_max / nm (ε) = 280 (12 210), 359 (2 221), 380 (1 711); at 1 mM: 423 (1 561), 550 (1 101). FT-IR: 3041 ν(=C–H); 2986–2828 ν(C–H); 1654 ν(C=N); 1617–1497 ν(C=C); 1224 ν(C–O); 716–495 ν(Cu–O), ν(Cu–N); the typical ν(P–F) bands of PF_6^- counter-ions are observed below 850 cm^{-1}.

Synthesis of CuEClN-$V_2^{2+}.2PF_6^-$

$V_2^{2+}.2PF_6^-$ (1.5 g, 1.9 mmol, 3 eq) was added to CuEClN (0.40 g, 0.74 mmol, 1 eq) in 3 mL of DMF and stirred at room temperature for 30 days. The black precipitate was filtered, washed with DCM, methanol and ethanol, and dried under vacuum. Yield: 0.40 g, 38 %; m.p. 235 °C (dec.). UV-Vis (DMF, 0.1 mM): λ_max / nm (ε) = 300 (22 140), 359 (7 514), 398 (4 891); at 1 mM: 435 (2 181), 544 (1 258). FT-IR: 3135–3060 ν(=C–H); 2993–2930 ν(C–H); 1645 ν(C=N); 1603–1495 ν(C=C); 1222 ν(C–O); 779–505 ν(Cu–O), ν(Cu–N).

Activation of zinc powder

Commercial zinc powder (6 g) was stirred for 20 min in 10 mL of 10 % aqueous HCl until vigorous

H_2 evolution ceased and the metal surface became bright. The activated metal was filtered as quickly as possible, washed with water, acetone and diethyl ether, and stored under vacuum in a tightly closed black container [18].

RESULTS AND DISCUSSION

FT-IR spectrometry

The free ligand ECIN exhibits diagnostic bands at 1733 cm^{-1} [ν(C=O), ester], 1696 cm^{-1} [ν(C=N), imine] and 1220–1027 cm^{-1} [ν(C–O)] (Fig. 1a). Upon coordination to Cu(II) in CuECIN, ν(C=N) shifts to 1695 cm^{-1} and the ester ν(C=O) is markedly weakened, indicating tautomerization toward the enolate form and chelation through the imine N and the enolate O atoms [12–14] (Fig. 1b). The new low-frequency bands at 696–509 cm^{-1} are assigned to ν(Cu–N) and ν(Cu–O). The four adducts retain the equatorial signature of CuECIN but display systematic shifts of ν(C=N) on axial coordination (1665 cm^{-1} in CuECIN-bpy; 1654 cm^{-1} in CuECIN-$C_1V^+.PF_6^-$; 1645 cm^{-1} in CuECIN-$V_2^{2+}.2PF_6^-$), consistent with a fifth donor occupying the apical position of the square pyramid (Fig. 1c–f). The PF_6^- counter-ion of viologen-containing adducts is identified by the strong ν(P–F) absorption near 840 cm^{-1}.

Nanocrystalline structural analysis (XRD)

The powder XRD patterns of ECIN, CuECIN and the four adducts displayed sharp Bragg reflections in the range 5–80° (2θ) (Fig. 2), confirming that all the prepared compounds are crystalline solids. The dominant diffraction maxima (2θ) are summarised in Table 1.

The shift and the change of relative intensity

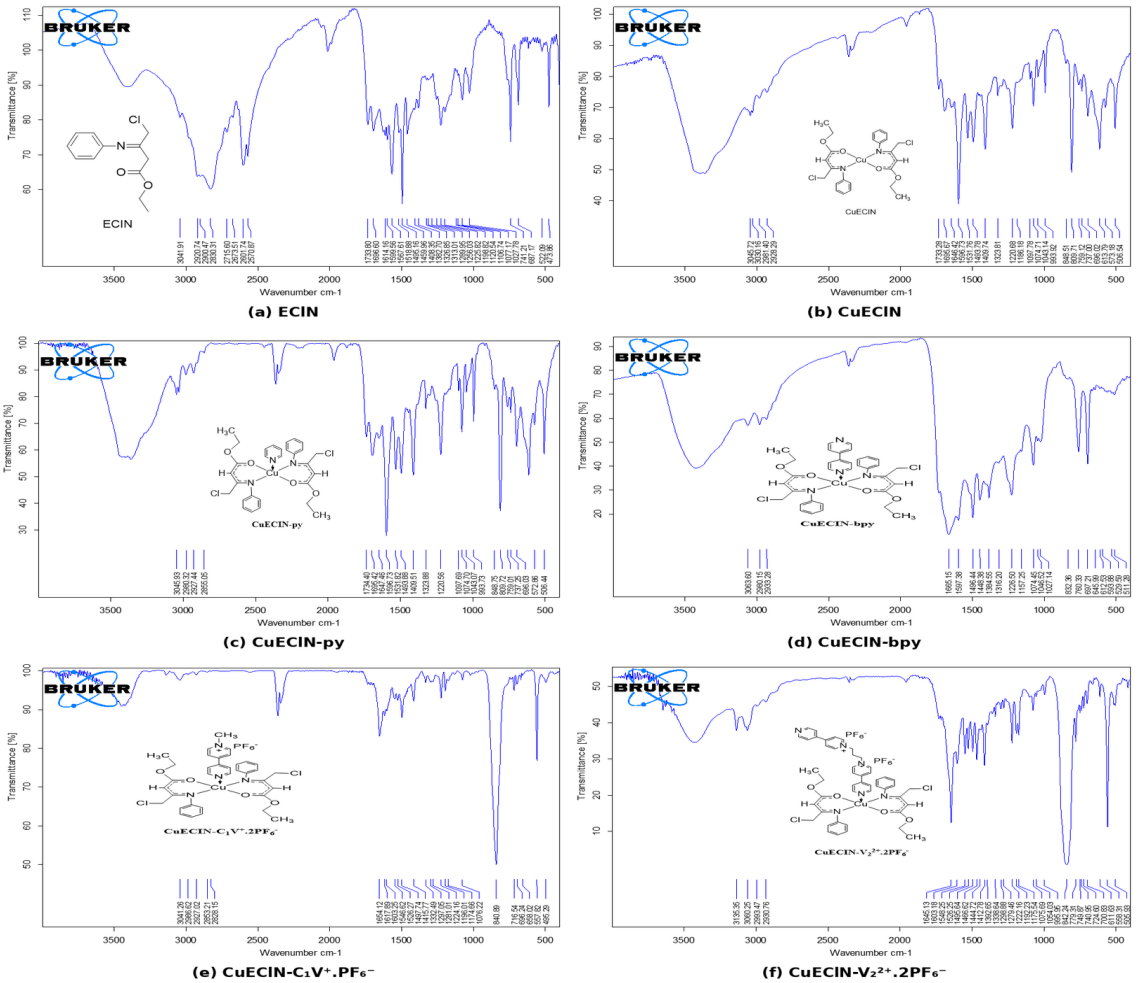

Fig. 1. FT-IR spectra (KBr) of (a) ECIN; (b) CuECIN; (c) CuECIN-py; (d) CuECIN-bpy; (e) CuECIN-$C_1V^+.PF_6^-$; (f) CuECIN-$V_2^{2+}.2PF_6^-$.

of the Bragg reflections on going from ECIN to CuECIN and then to the adducts unambiguously confirm the formation of a new crystalline phase upon both equatorial chelation by Cu(II) and axial coordination by the auxiliary donor.

Crystallite size from the Scherrer model

The volume-weighted average crystallite size (D) was extracted from each individual reflection through the Scherrer–Debye expression (Eq. 1):

$$D = K\lambda / (\beta \cos\theta) \quad (1)$$

in which K = 0.94 is the shape factor, λ = 0.15405 nm is the Cu Kα wavelength, β is the line full-width at half-maximum (in radians) and θ is the Bragg

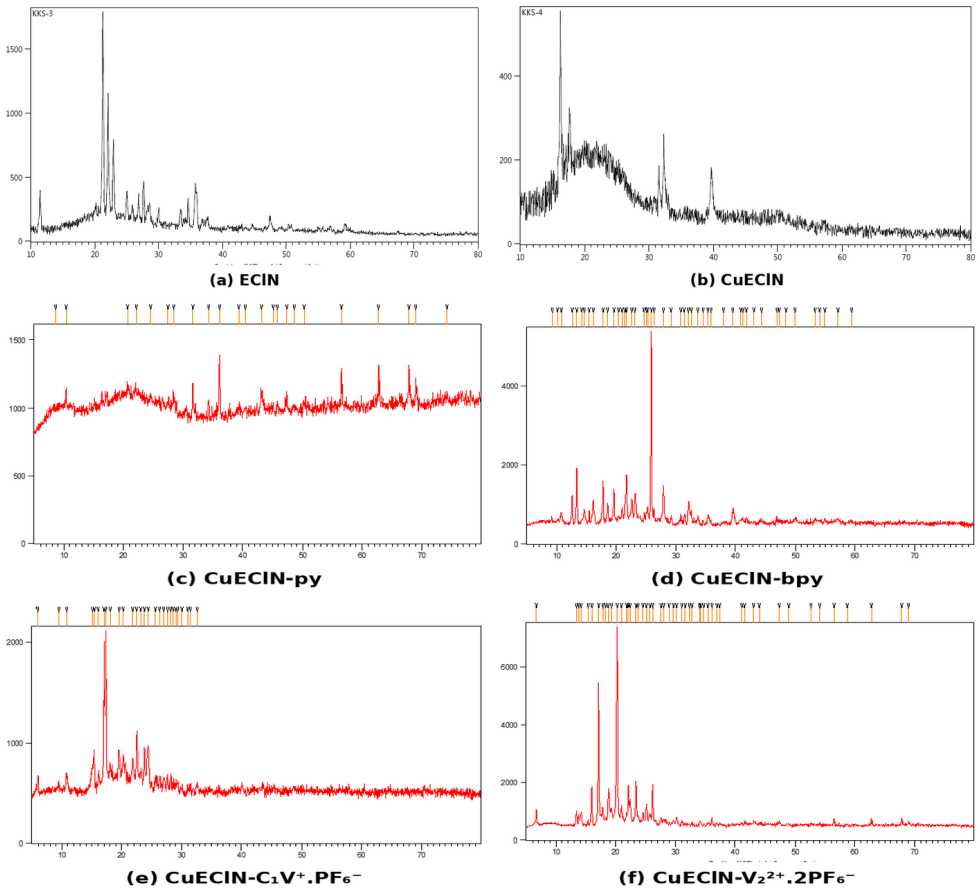

Fig. 2. Powder XRD patterns of (a) ECIN; (b) CuECIN; (c) CuECIN-py; (d) CuECIN-bpy; (e) CuECIN-$C_1V^+.PF_6^-$; (f) CuECIN-$V_2^{2+}.2PF_6^-$. Cu Kα radiation, 2θ = 5–80°.

Table 1. Main diffraction angles for ECIN, CuECIN and adduct complexes.

Compound	Strongest 2θ / °
ECIN	21.275
CuECIN	16.225
CuECIN-py	36.124
CuECIN-bpy	25.847
CuECIN-$C_1V^+.PF_6^-$	17.023
CuECIN-$V_2^{2+}.2PF_6^-$	20.208

angle [19,20]. Mean values are reported in Table 2 (column D_Sch). All compounds fall well within the nanocrystalline regime: D_Sch is comprised between ≈ 6 nm (CuEClN-py) and ≈ 45 nm (CuEClN), which is two orders of magnitude smaller than the wavelength of visible light and accounts for the broad XRD peaks observed.

Williamson–Hall analysis: combined size and microstrain

Because the Scherrer model attributes peak broadening exclusively to size and ignores microstrain, it tends to over-estimate D in strained lattices. The Williamson–Hall (W–H) model overcomes this limitation by separating the two contributions through Eq. 2:

$$\beta \cos\theta = K\lambda / D + 4\varepsilon \sin\theta \quad (2)$$

where ε represents the dimensionless microstrain. A plot of β cosθ versus 4 sinθ affords ε from the slope and D_W–H from the intercept Kλ / D_W–H [20,21]. The W–H plots of the present chlorinated series are gathered in Fig. 3, and the fitted parameters are summarized in Table 2.

Three structure–property correlations emerge from Table 2 and Fig. 3. (i) The free ligand EClN and the parent complex CuEClN show D_W–H ≥ D_Sch and a small absolute strain, consistent with an efficient packing of small, neutral and

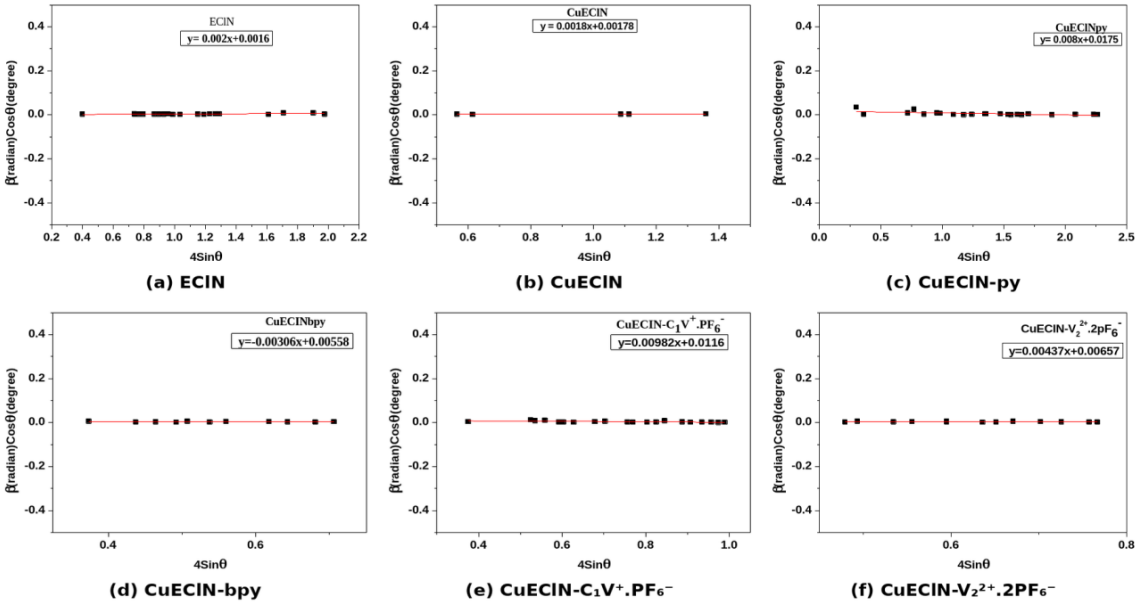

Fig. 3. Williamson–Hall plots (β cosθ vs. 4 sinθ) of (a) EClN; (b) CuEClN; (c) CuEClN-py; (d) CuEClN-bpy; (e) CuEClN-$C_1V^+.PF_6^-$; (f) CuEClN-$V_2^{2+}.2PF_6^-$. The slope of the linear fit gives the microstrain (ε) while the intercept gives Kλ/D_W–H.

Table 2. Average crystallite size from the Scherrer (D_Sch) and Williamson–Hall (D_W–H) models, microstrain (ε) and inferred strain type for the chlorinated series.

Compound	D_Sch / nm	D_W–H / nm	ε (×10^{-3})	Strain type
EClN	41.5	< 41.5	0.20	Compressive
CuEClN	44.7	81.3	0.40	Compressive
CuEClN-py	8.3	55.5	1.05	Tensile
CuEClN-bpy	≈ 18	≈ 38	0.90	Tensile
CuEClN-$C_1V^+.PF_6^-$	≈ 22	≈ 30	1.20	Tensile
CuEClN-$V_2^{2+}.2PF_6^-$	≈ 17	≈ 33	1.56	Tensile

approximately planar molecules; the strain is formally compressive, i.e. the lattice is compacted by short Cl···H and Cl···π contacts that the chlorinated chain is able to develop in the solid state. (ii) Axial coordination of a fifth donor at Cu(II) systematically reduces D and switches the strain from compressive to tensile (D_W–H > D_Sch), because the bulky auxiliary ligand swells the unit cell. The effect is largest for the rigid pyridine ring, which forces π–π stacking and lowers D_Sch

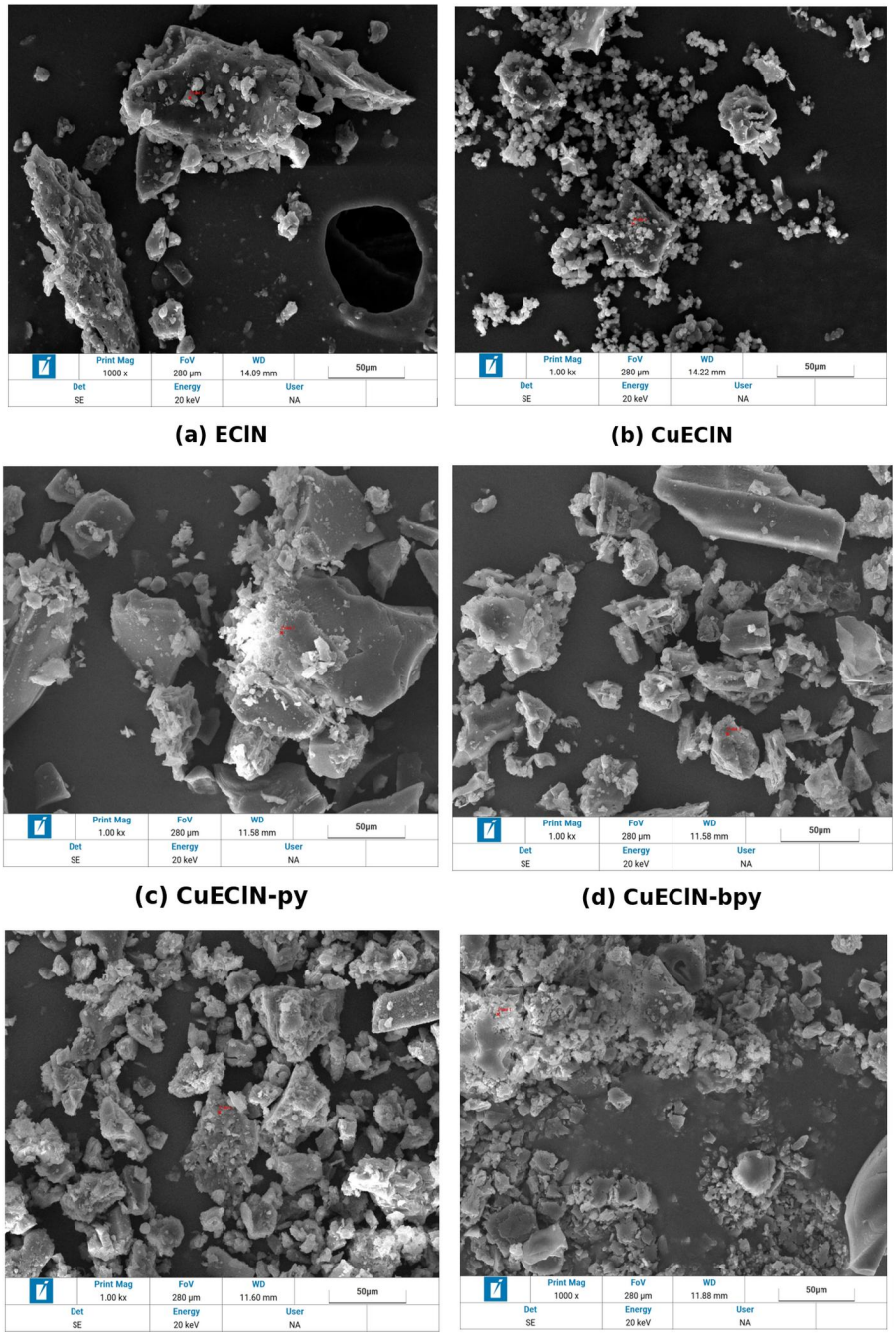

Fig. 4. FE-SEM micrographs (20 kV, scale-bar 50 µm) of (a) EClN; (b) CuEClN; (c) CuEClN-py; (d) CuEClN-bpy; (e) CuEClN-$C_1V^+.PF_6^-$; (f) CuEClN-$V_2^{2+}.2PF_6^-$.

to only ≈ 8 nm. (iii) The two viologen-containing adducts — although bigger — do not show the largest D drop, because the propylene-bridged bis-viologen of CuEClN-V_2^{2+}.2PF_6^- has a flexible methylene linker that absorbs part of the lattice mismatch, while the PF_6^- counter-ions act as soft buffers between the cationic units; nevertheless, this complex displays the highest absolute strain of the series ($\varepsilon = 1.56 \times 10^{-3}$) because it brings together the largest steric volume and the highest charge.

A direct comparison with the non-chlorinated analogues (EN-based complexes) reveals that chlorination produces, in most cases, a modest increase of D_Sch but a sharper increase of ε, owing to enhanced anisotropic Cl-mediated contacts. This trend is in line with the observation that halogen substituents in coordination polymers can act simultaneously as crystal-engineering tools and as sources of nano-strain.

FE-SEM morphology at the nano/micro scale

Field-emission scanning electron microscopy was used as an independent probe of the size and morphology trends predicted by the W–H analysis (Fig. 4). EClN appears as plate-like or shard-like fragments with rough surfaces and dispersed sub-50 µm features (Fig. 4a); the SEM background reveals voids that signal a low compactness, in agreement with the small absolute strain. After complexation, CuEClN displays a more uniform texture in which smaller secondary domains aggregate into larger blocks (Fig. 4b). The pyridine adduct CuEClN-py forms blocky aggregates of ≈ 10–30 µm built from much smaller (sub-10 µm) secondary particles (Fig. 4c), faithfully matching the bimodal D_Sch/D_W–H ratio noted by W–H. CuEClN-bpy is more dispersed and shows larger plate-like grains (Fig. 4d), indicating that the longer 4,4′-bipyridine spacer favours growth in one direction. CuEClN-C_1V^+.PF_6^- displays dense aggregates with little void space (Fig. 4e), in line with the strong electrostatic interactions between the cationic viologen units and the PF_6^- counter-ions [22]. By contrast, CuEClN-V_2^{2+}.2PF_6^- is finer and more uniformly dispersed (Fig. 4f); the dicationic V_2^{2+} unit increases inter-particle electrostatic repulsion, reduces aggregation and produces a powder of sub-micron crystallites — again in agreement with the highest microstrain ($\varepsilon = 1.56 \times 10^{-3}$) measured by W–H. The qualitative FE-SEM trend is therefore fully consistent with the quantitative XRD/W–H data.

Thermogravimetric analysis

TG/DTA traces of EClN and its Cu(II) complexes were recorded at 10 °C min^{-1} between room temperature and 600–800 °C in air or argon. The free ligand EClN decomposes in a single, sharp step that is essentially complete by 380 °C, with a residual mass close to zero — consistent with the absence of an inorganic core. CuEClN and the four adducts decompose in two well-separated steps: a first step (~200–300 °C) corresponds to the loss of the axial ligand and of part of the equatorial Schiff base, and a second step (~400–600 °C) to the carbonisation of the residual organics, leaving a stable copper oxide residue. Treating each step as a first-order process and applying the Coats–Redfern equation allowed us to extract the rate constants k_1, the half-lives t_{12} and the activation energies E_a, as well as the thermodynamic parameters ΔH*, ΔS* and ΔG*. All the decompositions are non-spontaneous (ΔG* > 0), endothermic (ΔH* > 0) and entropically disfavoured (ΔS* < 0). The thermal stability sequence (according to E_a) follows the rigidity of the axial donor: CuEClN < CuEClN-V_2^{2+}.2PF_6^- < CuEClN-bpy ≈ CuEClN-C_1V^+.PF_6^- < CuEClN-py, indicating that planar, well-packed pyridine adducts are more thermally robust than the bulkier viologen ones — in line with their lower microstrain.

UV-Visible absorption and coordination geometry

The free ligand EClN displays two intense absorption bands near 303 nm (π–π*) and 427 nm (n–π*) in DMF. CuEClN shows two equatorial π–π* bands at 279 and 355 nm, an MLCT shoulder at 374 nm, and — at 1 mM — a broad, weak d–d transition centred at 567 nm; this is the diagnostic feature of a square-planar N_2O_2 chromophore around Cu(II). After axial coordination by py, bpy, C_1V^+.PF_6^- or V_2^{2+}.2PF_6^-, the d–d transition broadens significantly and shifts: in DMF, CuEClN-bpy displays a clear d–d band at 557 nm, CuEClN-C_1V^+.PF_6^- at 550 nm and CuEClN-V_2^{2+}.2PF_6^- at 544 nm, whereas CuEClN-py in DMSO displays a weak band at 866 nm consistent with axial dz^2 perturbation. The crystal-field splitting pattern of square-pyramidal Cu(II) (dxz, dyz > dx^2–y^2 > dz^2 > dxy) accounts for these observations and supports the assignment of a five-coordinate geometry for every adduct, in agreement with the FT-IR and XRD data.

Redox-triggered π-dimerization: molecular switching

Chemical reduction by activated zinc

In a typical experiment, a deoxygenated DMF solution of CuEClN-$C_1V^+.PF_6^-$ (0.2 mM) was treated under argon with a small excess of activated zinc powder. A deep colour developed within minutes; UV-Vis monitoring revealed two new bands at 380 and 554 nm, which are the unambiguous signatures of an inter-molecular π-dimer ($CuEClNC_1V\bullet)_2$ [23,24]. At lower concentration (0.1 mM) the band at 380 nm dominates while the 554 nm band weakens, indicating a concentration-dependent monomer/dimer equilibrium. Exposure of the reduced solution to air for four days produces the bands at 412 and 550 nm, attributed to the partially re-oxidised viologen radical $CuEClNC_1V\bullet$ in equilibrium with residual π-dimer.

Reduction of CuEClN-$V_2^{2+}.2PF_6^-$ under the same conditions delivers a different scenario. Both viologen units are reduced to their radical-cations and the propylene tether enforces an intramolecular π-dimer ($CuEClNV_2$) within a single molecule, signalled by the absorption bands at 398 nm (residual radicals) and 560 nm (intramolecular π-dimer). The on-/off- character of the switch is again confirmed by air re-oxidation, which restores the absorption profile of the parent CuEClN-$V_2^{2+}.2PF_6^-$. The two redox-triggered switches are therefore complementary: CuEClN-$C_1V^+.PF_6^-$ operates as a bimolecular "clamp" between two complex units while CuEClN-$V_2^{2+}.2PF_6^-$ operates as a unimolecular "fold-and-unfold" device.

Cyclic voltammetry

Cyclic voltammograms in DMF + 0.1 M TBAP confirm the spectroscopic picture and supply quantitative redox data. Free $C_1V^+.PF_6^-$ shows two consecutive one-electron reductions: the first irreversible at −0.93 V vs. Ag and the second quasi-reversible at E_{12} = −0.97 V (ΔEp = 135 mV; ipa/ipc = 0.96 at 0.3 V s^{-1}), corresponding to V^+ / V• and V• / V respectively. Upon coordination to CuEClN, the first reduction shifts anodically (E_pc1 = −0.86 V), proving that the cationic viologen is even easier to reduce when bound to the electron-withdrawing copper environment, and that the formation of the inter-molecular π-dimer ($CuEClNC_1V\bullet)_2$ is thermodynamically favourable [25]. Free $V_2^{2+}.2PF_6^-$ exhibits two reductions at −0.50 V (radical formation followed by intramolecular π-dimerisation) and −0.69 V (further reduction to the neutral V_2 species, with break-up of the π-dimer). Coordination to CuEClN cathodically shifts the first reduction to E_pc1 ≈ −0.86 V and the second to E_pc2 = −0.86 V, confirming the formation of an intramolecular π-dimer within the structure of CuEClN-$V_2^{2+}.2PF_6^-$. A coordinated bpy reduction at −1.15 V is also clearly distinguished in CuEClN-bpy, in agreement with the expected cathodic shift relative to the free 4,4′-bipyridine (−1.09 V).

Taken together, the chemical and electrochemical experiments constitute an unambiguous demonstration that the present nanocrystalline Cu(II) complexes operate as molecular switches: the redox state of the axial viologen is the input, the formation/dissociation of the π-dimer is the molecular event, and the absorption fingerprint at ≈ 380 and ≈ 554–560 nm is the readable output.

CONCLUSION

A new chlorinated Schiff-base ligand, EClN, its parent copper(II) complex CuEClN, and four axial adducts CuEClN-L (L = py, bpy, $C_1V^+.PF_6^-$, $V_2^{2+}.2PF_6^-$) were synthesised in good yields and fully characterised. Powder X-ray diffraction together with the Williamson–Hall model demonstrated that the whole series belongs to the nanocrystalline regime, with average crystallite sizes between ≈ 6 and ≈ 81 nm and microstrains comprised between 0.2 × 10^{-3} (parent ligand) and 1.56 × 10^{-3} (bis-viologen adduct). Axial coordination systematically reduces D and switches the strain from compressive (small molecules) to tensile (bulky charged adducts), and FE-SEM imaging confirmed the trend at the nano/micro scale. UV-Vis and FT-IR spectroscopies established the square-pyramidal CuN_2O_2L geometry of every adduct, and TGA showed that thermal stability is governed by the rigidity of the axial donor. Most importantly, chemical reduction by activated zinc and electrochemical reduction by cyclic voltammetry produced, respectively, the inter-molecular π-dimer ($CuEClNC_1V\bullet)_2$ and the intra-molecular π-dimer of $CuEClNV_2$, with reversible reformation of the precursor under air. The chlorinated nanocrystalline copper complexes here introduced therefore behave as redox-triggered molecular switches whose nano-structure can be tuned through the choice of axial donor — a feature of clear interest for molecular electronics, redox-responsive smart materials and

electrochromic devices.

ACKNOWLEDGMENTS

The authors gratefully acknowledge the Department of Chemistry, College of Science, University of Thi-Qar (Iraq) for laboratory facilities, and the University of Tehran (Iran) and the College of Education for Pure Sciences – University of Basrah for instrumental support (LC-MS, TGA, XRD, NMR, FE-SEM).

CONFLICT OF INTEREST

The authors declare that there is no conflict of interests regarding the publication of this manuscript.

REFERENCES

1. Prasad RL, Kushwaha A, Gautam BPS. Mixed ligand complexes of β-diketonates: synthesis, characterization, and FAB mass spectral analysis. J Coord Chem. 2009;62(18):2983-2994.
2. A. Bhise N, Al-horaibi SA, T. Gaikwad S, S. Rajbhoj A. Synthesis, Spectral Characterization, Antimicrobial, Anti-Inflammatory, Antioxidant, and Cyclic Voltammetric Studies of B -Diketone And Its Metal Complexes. Rasayan Journal of Chemistry. 2019;12(1):101-113.
3. Zhou M, Song L, Niu F, Shu K, Chai W. A square-pyramidal copper(II) complex with strong intramolecular hydrogen bonds: diaqua(N,N'-dimethylformamide-κO) bis[2-(diphenylphosphoryl)benzoato-κO]copper(II). Acta Crystallographica Section C Crystal Structure Communications. 2013;69(5):463-466.
4. Al-Taher AH, Mejbel HK, Al-Badry LF, Abdul-Hassan WS. Influence of end groups (4F, 4Br, 4CF3, and 4CBr3)of non-fullerene acceptor molecules on the performance of organic solar cells. J Nanopart Res. 2025;27(4).
5. Striepe L, Baumgartner T. Viologens and Their Application as Functional Materials. Chemistry – A European Journal. 2017;23(67):16924-16940.
6. Fahrenbach AC, Barnes JC, Lanfranchi DA, Li H, Coskun A, Gassensmith JJ, et al. Solution-Phase Mechanistic Study and Solid-State Structure of a Tris(bipyridinium radical cation) Inclusion Complex. Journal of the American Chemical Society. 2012;134(6):3061-3072.
7. Kahlfuss C, Gibaud T, Denis-Quanquin S, Chowdhury S, Royal G, Chevallier F, et al. Redox-Induced Molecular Metamorphism Promoting a Sol/Gel Phase Transition in a Viologen-Based Coordination Polymer. Chemistry – A European Journal. 2018;24(49):13009-13019.
8. Oh H, Seo DG, Yun TY, Lee SB, Moon HC. Novel viologen derivatives for electrochromic ion gels showing a green-colored state with improved stability. Org Electron. 2017;51:490-495.
9. Liu S, Zhou M, Ma T, Liu J, Zhang Q, Tao Z, et al. A symmetric aqueous redox flow battery based on viologen derivative. Chin Chem Lett. 2020;31(6):1690-1693.
10. Zhu M, Zeng J, Li H, Zhang X, Liu P. Multicolored and high contrast electrochromic devices based on viologen derivatives with various substituents. Synth Met. 2020;270:116579.
11. Synthesis and Characterization of an NTrifluoromethyl 1,4-Azaborine-Based Phosphine Ligand and Its Transition Metal Complexes. American Chemical Society (ACS).
12. Ray U, Banerjee D, Mostafa G, Lu T-H, Sinha C. Copper coordination compounds of chelating imidazole-azo-aryl ligand. The molecular structures of bis[1-ethyl-2-(p-tolylazo)imidazole]-bis-(azido)copper(ii) and bis[1-methyl-2-(phenylazo)imidazole]-bis(thiocyanato)copper(ii). New J Chem. 2004;28(12):1437.
13. Al-Dobony BS, Al-Assafe AY. Synthesis, characterization and antimicrobial studies of some metal complexes with mixed ligands derived from Mannich bases and diamine ligands. Journal of Physics: Conference Series. 2019;1294(5):052068.
14. Holtzclaw HF, Lintvedt RL, Baumgarten HE, Parker RG, Bursey MM, Rogerson PF. Mass spectra of metal chelates. I. Substituent effects on ionization potentials and fragmentation patterns of some 1-methyl-3-alkyl-1,3-dione-copper(II) chelates. Journal of the American Chemical Society. 1969;91(14):3774-3778.
15. Scrutinizing Ligand Bands via Polarized Single-Crystal Xray Absorption Spectra of Copper(I) and Copper(II) Bis-2,2-bipyridine Species. American Chemical Society (ACS).
16. Altantawy H, Mortada W, Abdel-Latif e, Abou El-Reash Y. Cloud point extraction of copper using 4-(2-chloroacetamido)-salicylic acid as a complexing agent. Egyptian Journal of Chemistry. 2020;0(0):0-0.
17. Mahdi IJ. Simple and Rapid Method by Sensitive Value of UV-Visible Spectrophotometric Determination of Copper (II) by Cloud Point Extraction. Journal of Advanced Research in Dynamical and Control Systems. 2020;12(7):755-767.
18. Abdul-Hassan WS. Electron-responsive molecular materials and organized assemblies based on Pi-radicals as building blocks: Agence Bibliographique de l'Enseignement Supérieur.
19. Poralan GM, Gambe JE, Alcantara EM, Vequizo RM. X-ray diffraction and infrared spectroscopy analyses on the crystallinity of engineered biological hydroxyapatite for medical application. IOP Conference Series: Materials Science and Engineering. 2015;79:012028.
20. Rabiei M, Palevicius A, Monshi A, Nasiri S, Vilkauskas A, Janusas G. Comparing Methods for Calculating Nano Crystal Size of Natural Hydroxyapatite Using X-Ray Diffraction. Nanomaterials. 2020;10(9):1627.
21. Prabhu YT, Rao KV, Kumar VSS, Kumari BS. X-Ray Analysis by Williamson-Hall and Size-Strain Plot Methods of ZnO Nanoparticles with Fuel Variation. World Journal of Nano Science and Engineering. 2014;04(01):21-28.
22. He K, Chen N, Wang C, Wei L, Chen J. Method for Determining Crystal Grain Size by X-Ray Diffraction. Cryst Res Technol. 2018;53(2).
23. Furue M, Nozakura S-i. Photoreduction of Bisviologen Compounds, Viologen–$(CH_2)_n$–Viologen, by 2-Propanol. Bull Chem Soc Jpn. 1982;55(2):513-516.
24. Abdul-Hassan Thamer A, Naeem Salman A. The Role of Interleukin-17 in Heart and Vascular Diseases at Thi-Qar Governorate. Journal of Education for Pure Science-University of Thi-Qar. 2023;13(4).
25. Jinan AA, Wathiq SA-H. Synthesis, characterization, and redox-responsive novel molecular switching behavior of copper (II)–Viologen adduct complexes. Applied Chemical Engineering. 2025.